In Vivo Two-Photon Fluorescence Kinetics of Primate Rods and Cones

Robin Sharma,[1,2] Christina Schwarz,[2] David R. Williams,[1–3] Grazyna Palczewska,[4] Krzysztof Palczewski,[5] and Jennifer J. Hunter[2,3]

[1]The Institute of Optics, University of Rochester, Rochester, New York, United States
[2]Center for Visual Science, University of Rochester, Rochester, New York, United States
[3]Flaum Eye Institute, University of Rochester, Rochester, New York, United States
[4]Polgenix, Inc., Cleveland, Ohio, United States
[5]Department of Pharmacology, Cleveland Center for Membrane and Structural Biology, School of Medicine, Case Western Reserve University, Cleveland, Ohio, United States

Correspondence: Robin Sharma, University of Rochester, Center for Visual Science, 601 Elmwood Avenue, BOX 319, Rochester, NY 14642, USA;
rsharma@optics.rochester.edu.

Submitted: August 13, 2015
Accepted: January 5, 2016

Citation: Sharma R, Schwarz C, Williams DR, Palczewska G, Palczewski K, Hunter JJ. In vivo two-photon fluorescence kinetics of primate rods and cones. *Invest Ophthalmol Vis Sci*. 2016;57:647–657. DOI:10.1167/iovs.15-17946

Purpose. The retinoid cycle maintains vision by regenerating bleached visual pigment through metabolic events, the kinetics of which have been difficult to characterize in vivo. Two-photon fluorescence excitation has been used previously to track autofluorescence directly from retinoids and pyridines in the visual cycle in mouse and frog retinas, but the mechanisms of the retinoid cycle are not well understood in primates.

Methods. We developed a two-photon fluorescence adaptive optics scanning light ophthalmoscope dedicated to in vivo imaging in anesthetized macaques. Using pulsed light at 730 nm, two-photon fluorescence was captured from rods and cones during light and dark adaptation through the eye's pupil.

Results. The fluorescence from rods and cones increased with light exposure but at different rates. During dark adaptation, autofluorescence declined, with cone autofluorescence decreasing approximately 4 times faster than from rods. Rates of autofluorescence decrease in rods and cones were approximately 4 times faster than their respective rates of photopigment regeneration. Also, subsets of sparsely distributed cones were less fluorescent than their neighbors immediately following bleach at 565 nm and they were comparable with the S cone mosaic in density and distribution.

Conclusions. Although other molecules could be contributing, we posit that these fluorescence changes are mediated by products of the retinoid cycle. In vivo two-photon ophthalmoscopy provides a way to monitor noninvasively stages of the retinoid cycle that were previously inaccessible in the living primate eye. This can be used to assess objectively photoreceptor function in normal and diseased retinas.

Keywords: ophthalmic imaging, photoreceptors, visual cycle, pigment regeneration

It has been known since the 19th century that light is captured by visual pigments in the outer segments (OS) of photoreceptor cells.[1,2] Experiments performed by Wald[3] and Hubbard and Wald[4] revealed that visual pigment molecules are composed of two components, namely an opsin protein and a chromophore, 11-*cis*-retinal.[3,4] Upon absorption of a photon by the pigment, the chromophore isomerizes to all-*trans*-retinal, which subsequently is released from the opsin through a series of intermediate steps.[5] This initiates the regeneration of photopigment through the visual (retinoid) cycle.[6] During regeneration, all-*trans*-retinal is reduced to all-*trans*-retinol,[7] which subsequently is transferred from OS to RPE cells[8] and also to Müller cells, which contribute to photopigment regeneration in cones.[9–12] Measurement of the photopigment regeneration rate has been used as a marker for disease in photoreceptors and the RPE.[13] To monitor pigment regeneration directly in the living human eye, rhodopsin densitometry has been used.[14–16] However, interpretation of densitometry data is complicated by the contribution of intrinsic optical signals to observed changes in reflectance, which currently are inexplicable within the current model of pigment regeneration kinetics.[17–19]

Retinoid absorption and fluorescence properties also can be exploited to track retinoid concentrations following light exposure. Ultraviolet (UV) light has been used to excite autofluorescence from all-*trans*-retinol to track the visual cycle in isolated cells from various animal models.[20–23] However, different species metabolize retinoids at different rates, complicating direct comparisons of regeneration rates in animal versus human retina.[13] The physiology and anatomy of nonhuman primate retina, particularly old-world monkeys,[24] is similar to that in humans, making them an appropriate animal model. However, little is known about the kinetics of intermediate stages of the retinoid cycle in living primates. For in vivo imaging, optical techniques relying on single-photon fluorescence excitation of retinoids cannot be used in primates because UV light is outside the spectral barrier for transmission through the optics of the eye.[25]

Two-photon fluorescence (TPF) imaging[26,27] overcomes these spectral barriers and offers the potential for a noninvasive

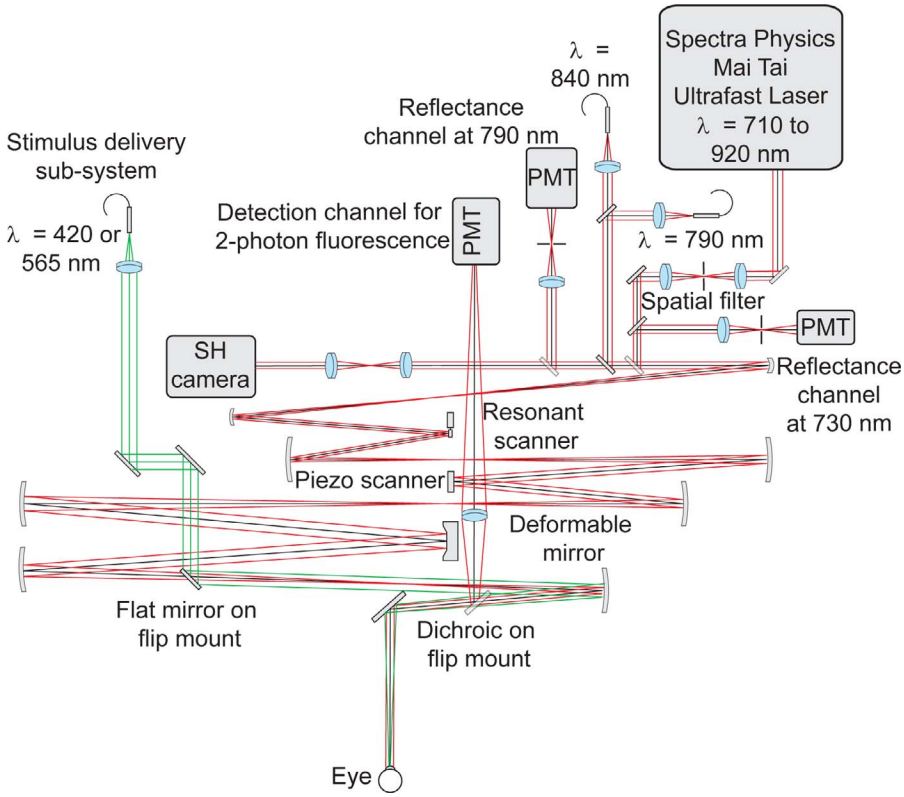

Figure 1. Layout of the TPF-AOSLO. Multiple light sources were used for different purposes (840 nm light for wavefront sensing, 790 nm light for reflectance imaging, 730 nm light for TPF excitation and reflectance imaging). Light emitted by the ultrashort pulsed laser was directed through a spatial filter, collected through a collimating lens, and then routed through a beam splitter and directed into the AOSLO system through a custom dichroic mirror. Within the AOSLO, light reflected off of multiple spherical mirrors, two scanners, and a deformable mirror, and passed through a dichroic mirror before finally being diverted into the eye by a fold mirror. Electronically controlled flip mirrors regulated the delivery of full-field stimuli to the eye. During two-photon imaging, the emitted fluorescence was reflected off the dichroic mirror and collected by a PMT. Two additional PMTs were used for collecting backscattered light in the confocal mode at 730 and 790 nm.

approach for studying visual function at a cellular scale in the living eye. Previously, we have demonstrated TPF imaging of photoreceptors and RPE in the mouse eye[28–31] and an increased fluorescence over time in photoreceptors of the macaque.[32] From the point of view of translating this technique to human imaging, its use depends on identifying and characterizing the dominant source(s) of time-variable autofluorescence in primate eyes, which could emanate from one or more among a list of candidate fluorophores. Examples include retinoids, NAD(P)H, FAD, collagen, elastin, lipofuscin, and perhaps others.[33–35] Previous reports on autofluorescence from the retina[20,21,29,36] have identified all-*trans*-retinol as the dominant source of time-variable fluorescence in mammalian photoreceptors. To investigate this hypothesis in living primates, we used a new generation two-photon ophthalmoscope to characterize the TPF responses from individual photoreceptors under different conditions of light and dark adaptation.

Methods

Animal Preparation

Three nonhuman primates, one male *Macaca fascicularis* monkey (20 years old) and two female *Macaca mulatta* monkeys (4 and 16 years old), were studied in these experiments. All subjects in this study were handled in accordance with the protocols approved by the University of Rochester's committee for animal research and in adherence with the ARVO Statement for the Use of Animals in Ophthalmic and Vision Research. Subjects were sedated with ketamine (<20 mg/kg) and Valium (0.25 mL/kg), and once intubated, were kept under a constant influx of isoflurane (ranging from 1%–5%). A paralytic dose of vecuronium (60 μg/kg/h) was administered for a maximum period of 6 hours to reduce involuntary eye-drifts and breathing was maintained with a ventilator. Animals were imaged by placing them in a sternal position on a stereotaxic cart with a singular gimbal focus of rotation and the eye was placed at this location for imaging. The imaged eye was held open with a lid speculum. A contact lens coated with Genteal (Alcon, Fort Worth, TX, USA) was used to correct for base refractive error and maintain corneal hydration for the duration of each experiment.

TPF Adaptive Optics Scanning Light Ophthalmoscope (TPF-AOSLO)

A custom TPF-AOSLO was designed and built to optimize the efficiency of TPF imaging in the living monkey eye. The system design was similar to previously reported instruments[37,38] and the layout is shown in Figure 1. A resonant scanner (Electro-Optical Products Corp., Fresh Meadows, NY, USA) operating at 13.6 kHz was used for raster scanning in the horizontal direction and a 2-axis tip/tilt mirror (S-334.2SL; Physik Instrumente, Karlsruhe, Germany) was used for scanning in the vertical direction. A deformable mirror was used for

adaptive optics correction (DM97-15; ALPAO SAS, Grenoble, France). The scanners and deformable mirror were placed in planes that were conjugate to the eye's entrance pupil. All optical elements in the beam path within the TPF-AOSLO were silver coated for optimal performance in the infrared regime. The Hartmann-Shack scheme was used for wavefront sensing. A lenslet array (203-μm pitch, 7.8-mm focal length per lenslet; Adaptive Optics Associates, Cambridge, MA, USA) was placed in front of a CCD camera (Rolera XR; QImaging, Surrey, BC, Canada) and was located in a plane that was conjugate to the eye's entrance pupil plane. A laser diode (LD) emitting quasi-monochromatic light at 840 nm (QPhotonics, Ann Arbor, MI, USA) was used as the wavefront sensing beacon.

Raster-scanned images of the retina were collected through multiple detection channels.

1. Light reflected or scattered back from a superluminescent diode (SLD) operating at a central wavelength of 790 nm (Superlum, Cork, Ireland) was descanned through the system and collected through a confocal pinhole (2.5 airy-discs in diameter) by a photomultiplier tube (PMT H7422-50; Hamamatsu Corporation, Shizuoka-Ken, Japan).
2. A pulsed laser (Mai Tai XF-1; Newport Spectra-Physics, Santa Clara, CA, USA) was used as the TPF excitation source. This laser had a tunable central wavelength (710–920 nm). All data reported here were collected at λ_{ex} = 730 nm. At this central wavelength, the laser emitted pulses of pulse-width <55 fs at 80 MHz repetition rate. A pair of prisms on motorized mounts was used for lower order dispersion compensation (DeepSee, Newport Spectra-Physics). The beam emitted from the laser was focused through a spatial filter and collimated with an achromatic doublet lens. Then, it was coupled with light from the SLD and LD with a custom dichroic mirror (Chroma Technology Corp., Bellows Falls, VT, USA) and diverted into the TPF-AOSLO and eventually the eye.

   Emitted TPF was collected in a nondescanned manner by diverting all the light exiting the eye in the visible wavelength range (400–665 nm) with a dichroic mirror (FF665-Di02; Semrock, Rochester, NY, USA). This light was collected by a lens and imaged on the surface of the detector (PMT H7422-40; Hamamatsu Corporation) placed at a plane conjugate to the pupil of the eye. Emission was collected between 400 and 550 nm with three filters; two filters with transmission band from 400 to 680 nm (ET680SP-2P8; Chroma Technology Corporation), and an additional filter with a transmission window from 400 to 550 nm (E550sp-2p; Chroma Technology Corporation).
3. In addition to serving as the two-photon excitation light source, backscattered light from the Mai Tai XF-1 laser at 730 nm was descanned through the system and collected through a confocal pinhole (2.2 airy-discs in diameter) with a photomultiplier tube (PMT H7422-50; Hamamatsu Corporation) to generate reflectance images of the retina.

Output photocurrents from reflectance and fluorescence channel PMTs were converted to voltage and amplified by transimpendance amplifiers (HCA-10M-100K; FEMTO Messtechnik GmbH, Berlin, Germany) and custom-built inverting amplifiers. These signals were digitized through an analog to digital convertor built into a FPGA card (Xilinx, Inc., San Jose, CA, USA). All images reported herein were collected with 7.5 mm diameter beam incident at the pupil of the eye. Compared to commercially available two-photon microscopes, resolution of this two-photon ophthalmoscope was limited by the numerical aperture of the monkey eye and the theoretically estimated axial resolution was >30 μm for 730 nm.[39]

A stimulus delivery subsystem was incorporated into the TPF-AOSLO to deliver stimuli in Maxwellian view (full field, nonscanning) using electronically controllable flip mirror mounts (shown in Fig. 1) to bleach a circular retinal area of approximately 3.2° in diameter. Light emitting diodes (LEDs) at two different wavelengths were used; at 565 and 420 nm. To divert stimuli into the eye, two flip mirrors were activated simultaneously; a fold mirror on a flip mount (located between the last two mirrors in the TPF-AOSLO) was flipped into position and the dichroic used for emission collection (located between the last mirror and the eye) was flipped out of position. In this arrangement, the retina could never be exposed simultaneously to the Ti:Sapphire laser and light from the LEDs, and consequently TPF emission could not be recorded during full-field stimulation.

Imaging Conditions

Bleaching by the Imaging Beam. Even though 730 nm light used for TPF excitation is outside the conventionally accepted visible spectrum, it can stimulate vision.[40,41] To study the effects of stimulation from the imaging light alone, subjects initially were dark adapted for 30 to 35 minutes. At the end of the dark adaptation interval, the imaging beam was diverted into the eye. Photoreceptor autofluorescence was tracked for over 2 minutes while the retina adapted to stimulation from the imaging light (depicted in Fig. 2a). At 730 nm, relative to the peaks of their normalized spectral sensitivities, rods are almost 1 log unit less sensitive than M cones, and almost 2 log units less sensitive than L cones.[42,43] While we do not have adequate knowledge of the two-photon action spectrum for photoisomerization of photopigments, at this wavelength, the likelihood of stimulation by two-photon absorption is lower than single-photon absorption.[41] To minimize the disparity in the photon catch rates (and consequently the rate of bleach) between different photoreceptor types, adaptation of rods to light was studied at higher incident power (7 mW at the pupil), while light adaptation in cones was studied at lower light levels (750 μW at the pupil) as well as at high light levels (7 mW at the pupil). Photopigment density was calculated for the steady state illumination condition using the formalism described by Mahroo and Lamb.[44]

Recovery to Dark-Adapted Levels. In rhodopsin densitometry, the retina first is subjected to visual stimulation and subsequently, photopigment density is measured during regeneration in the dark.[15,45] Comparison of time course of TPF with photopigment regeneration kinetics would be instructive but direct measurements of photoreceptor autofluorescence during dark adaptation are complicated because the imaging beam at 730 nm stimulates the retina. To overcome this unwanted stimulation, the following experimental protocol was used (as depicted in Fig. 2b):

1. Multiple full-field bleaching exposures were delivered to the retina at 565 nm for 3 to 5 seconds. The approximate fractions of photopigments bleached due to visible stimuli were estimated using pigment depletion kinetics for short bleaches[46] and spectral sensitivity data from Baylor[42,43] and are listed in Table 1
2. After each such exposure, the retina was allowed to recover for variable periods in the dark (Δt_{dark}) ranging from 0 to 30 minutes, selected in a random order.
3. After each such recovery period, TPF was recorded; to investigate light adaptation to the TPF excitation beam,

Investigative Ophthalmology & Visual Science

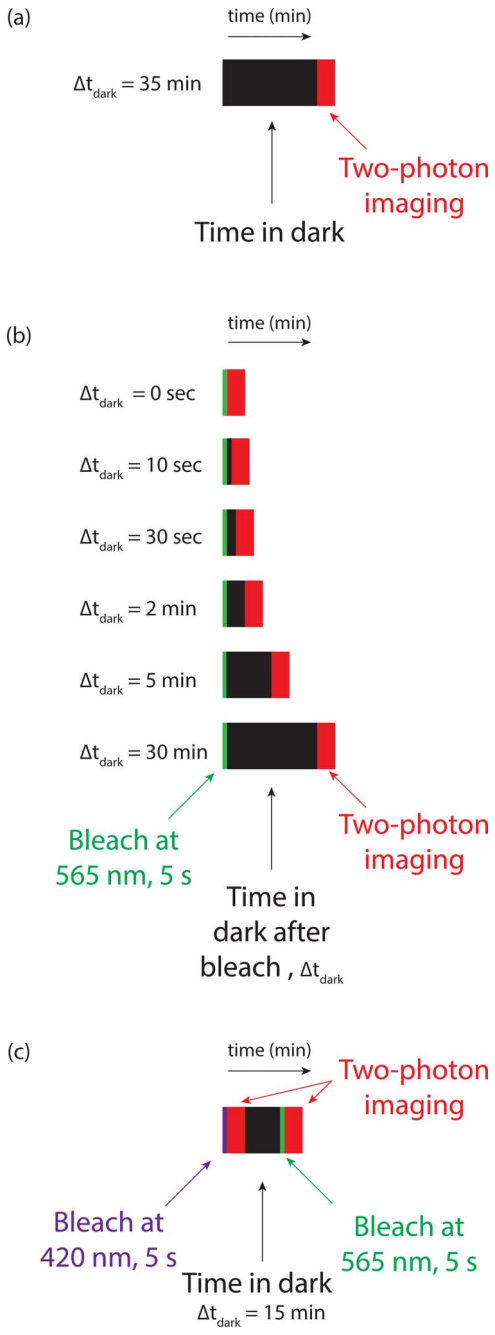

Figure 2. Two-photon imaging protocol used for studying adaptation of the retina to differing conditions of light exposure and darkness. (**a**) Paradigm used for studying adaptation responses to imaging beam. Retinas were initially dark-adapted for >30 minutes and then exposed to incident light. (**b**) Imaging conditions used for measuring dark adaptation responses over several imaging trials. Retinas were repeatedly bleached using a full-field stimulus and TPF was recorded after waiting for variable periods of time in the dark as shown. (**c**) Imaging protocol used for revealing S cone mosaic.

autofluorescence was tracked for 2 minutes after every such dark interval.

To facilitate interpretation of in vivo TPF data, pigment regeneration recovery curves during dark adaptation were calculated using the model developed by Mahroo, Lamb, and Pugh,[13,44] hereafter referred to as the MLP model.

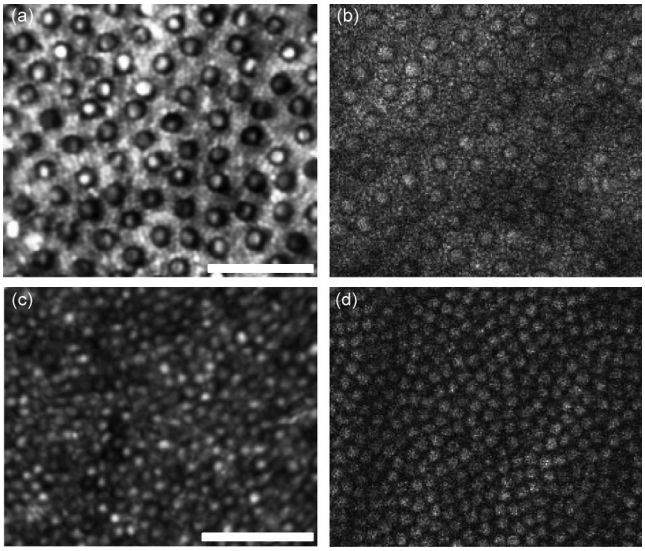

Figure 3. Photoreceptor mosaic imaged using TPF-AOSLO. (**a**) Reflectance image of photoreceptors collected through conventional backscattered confocal imaging modality in the peripheral retina at 8.75 mm temporal to the fovea. (**b**) Two-photon autofluorescence image of the same cells shown in (**a**). For a single frame, 0.0017 photons per pixel were collected on average and 3200 frames were added to generate these images. Individual rods were also visible in reflectance as well as fluorescence images. (**c**) Confocal reflectance image of photoreceptors at a retinal location approximately 1.2 mm inferior to the fovea and (**d**) the corresponding two-photon image collected at the same location. For a single frame, 0.0007 photons per pixel were collected on average and 3200 frames were added to generate the image. Images were contrast stretched for visual display. Apart from the imaging light at 730 nm, no external bleach at visible wavelengths was delivered before or during the recording of these data. *Scale bars*: 50 μm.

$$P(t) = 1 - K_m W\left\{\frac{B}{K_m}\exp\left(\frac{B}{K_m}\right)exp\left(-\frac{1+K_m}{K_m}vt\right)\right\},$$

where $P(t)$ is the quantity of photopigment at time t, K_m is the Michaelis constant, $W(x)$ is the Lambert W function, B is the initial fraction of bleached pigment, and $v = K_m/(1+K_m)\tau$, where τ is the regeneration time constant and v is related to the initial rate of rhodopsin regeneration. The parameters v and K_m used in this model were measured previously by retinal densitometry in two of the three animals used in this study and estimated by curve fitting to be 0.067 minutes^{-1} and 0.2.[19]

Adaptation to Spectrally Dissimilar Stimuli. To investigate the dependence of TPF on the spectra of bleaching light, fluorescence was recorded after bleaching the same cells at two different wavelengths, in addition to the stimulation from the imaging light. The retina initially was exposed to light at 420 nm (>90% of all cone pigments bleached[43]) and fluorescence was recorded immediately after bleach. After 15 minutes in the dark, the same location in the retina was stimulated at 565 nm (>90% M and L cone pigments bleached; <25% S cone pigments bleached[43]) and fluorescence was captured right after the bleach (depicted in Fig. 2c).

Image Analysis and Processing

Based on the imaging protocols described above, light and dark adaptation curves were measured from TPF videos. These videos were captured at frame rates of 20 or 22.5 Hz through custom software at a pixel clock rate of 35 MHz. Frame size was 512 lines along the direction of the slow scanner, which

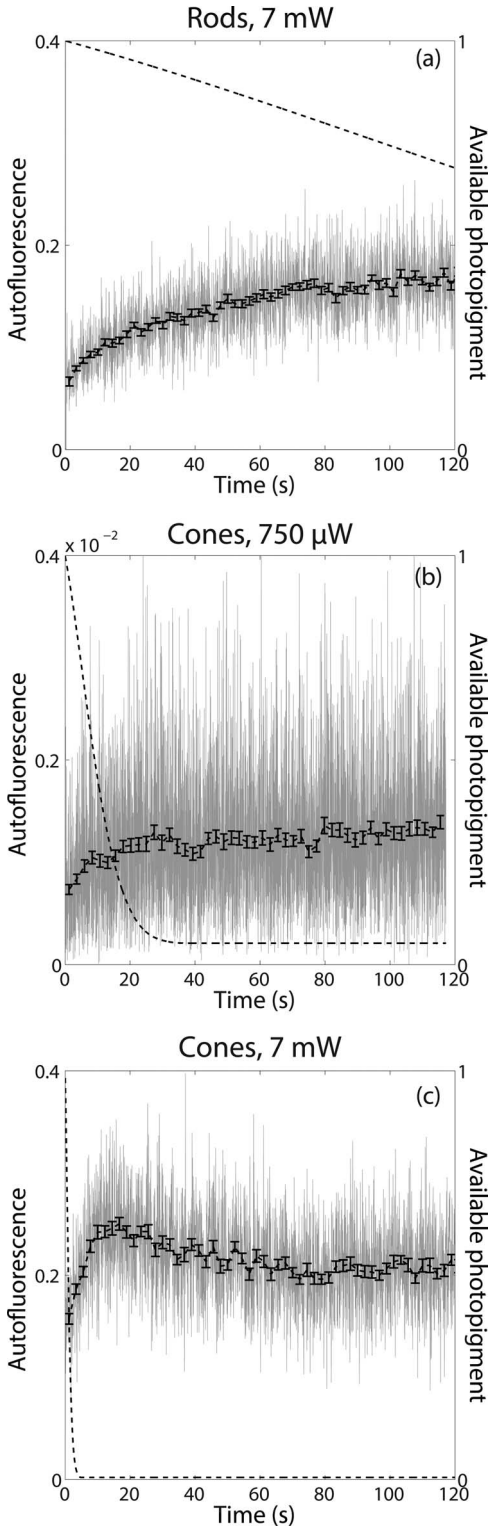

Figure 4. Adaptation responses of the retina from exposure to imaging light are shown. Raw data collected at frame rate are plotted in the background in *gray* and data binned over approximately 2-second intervals have been overlaid in *black* for display purposes. *Error bars*: SEM for each bin. Curves depicting the expected time course of photopigment density have been added to each figure. These were calculated using the formulae provided by Mahroo and Lamb.[44] (**a**) Time course of TPF captured from rods after 35 minutes of dark adaptation at 3.4 mm superior and temporal relative to the center of the foveal avascular zone. (**b**) Two-photon fluorescence response from cone photoreceptors after 35 minutes in dark at 750 µW incident light

had a linear motion range, and anywhere from 656 to 728 pixels along the direction of the fast scanner, which had a sinusoidal motion range. Videos were acquired by multiple channels simultaneously. Light and dark adaptation responses were extracted from raw data collected in this manner through a series of steps.

1. Sinusoidal motion of the resonant scanner was corrected during postprocessing by measurement and application of a transformation matrix to equalize the size of all pixels across the field. Residual motion artifacts in the videos were corrected with customized software by measuring interframe motion across all frames within high contrast reflectance videos with respect to a user-specified reference frame. These values then were used appropriately to displace all other frames in the reflectance video and subsequently the same corrections were applied to corresponding fluorescence videos that were acquired simultaneously to generate desinusoided and registered videos that were used for all analyses.[47]
2. Registered images of photoreceptors acquired in confocal reflectance mode were used to manually mark the X-Y coordinate locations of the center of all cone photoreceptors visible within the field of view. Shifts between the reflectance and fluorescence images, if any, were determined through normalized full-frame cross-correlations to calculate the coordinate locations for the corresponding cones in fluorescence images.
3. A custom MATLAB script was used to create circular masks centered at each cone in an image to selectively extract fluorescence only from the central portion of cone photoreceptors. The mask size was chosen to be smaller than the size of the cones by visual inspection. An inverted version of the mask used for cones was applied to the same videos to extract fluorescence kinetics from rods. These inverted masks were created to eliminate fluorescence from cones, and were larger than the cones in the image. Areas within the imaging field that might include blood vessel shadows or unmarked cones were manually masked out. These masks were applied to each frame in the desinusoided, registered videos to track fluorescence from cones and rods separately. By plotting the fluorescence intensity versus time during image acquisition, the adaptation to stimulation from imaging beam was quantified.
4. To generate the dark adaptation curves, the intercept at time $t = 0$ seconds, was estimated by linear curve fitting of the first 5 seconds of raw data to characterize the initial TPF responses from photoreceptors as a function of time in the dark after a bleach. Additionally, an exponential fit to the raw data was used to estimate the plateau value for the time course of TPF. The reasons for curve fitting the same data with a straight line and an exponential fit are as follows. Absolute fluorescence signals can be affected over time by external factors, such as contact lens dehydration or ocular pupil decentration. During experiments, videos were recorded from the same retinal location across several hours, and to nullify the impact of these external factors, the

←
recorded 0.6 mm nasal relative to the center of the foveal avascular zone. (**c**) Two-photon fluorescence response from cone photoreceptors after 30 minutes in dark at 7 mW incident light at a location 4.86 mm superior and temporal relative to the center of the foveal avascular zone. Parameters used for calculating pigment density of cones: $\sigma =$ 2.9e-7,[45,64] $\nu = 0.0083$,[44] $K_m = 0.2$,[44] $I = 7$ mW or 750 µW, and for rods: $\sigma =$ 1e-7,[46] $\nu = 0.0011$,[19] $K_m = 0.2$,[44] $I = 7$mW.

Investigative Ophthalmology & Visual Science

Table 1. Summary of Data on TPF-Based Kinetics of Rods and Cones During Dark Adaptation Collected in Three Different Animals

Subject, Number	Location from Fovea, mm	Imaging Light Level, mW	Bleach Light Level, μW (Fraction of Pigment Bleached, %)	Time Constant, min	R^2 for Fit
Rods					
526	4.86 S, T	7	66 (>90)	1.78	0.9873
734	3.4 S, T	7	71 (>90)	1.34	0.9699
406	2.43 I, T	7	56 (>90)	1.82	0.9706
734	2.9 S	7	58 (>90)	3.65	0.8378
406	3 I	3.5	6.8 (>50)	4.15	0.9722
734	3 T	4	6.75 (>50)	1.78	0.9873
406	1.8 I, N	0.78	6.8 (>50)	0.64	0.9753
406	1.5 N	0.78	6.8 (>50)	1.05	0.9747
Cones					
734	0.729 N	0.75	6.75 (>85)	0.28	0.9271
406	<1 S	0.765	6.35 (>85)	0.5811	0.8788
406	<1 I	0.765	6.35 (>85)	0.6703	0.6556

Raw data were fit to exponential functions $f(x) = a^*exp(-bx) + c$. This table lists the retinal eccentricities with respect to the center of the foveal avascular zone at which experiments were conducted, light levels used for full-field bleach at 565 nm, and the calculated fraction of bleached pigment under scotopic and photopic regimens, along with the light levels used for two-photon excitation at the eye's pupil (over 7.5 mm diameter). Two major results from the curve fit, namely the time constants and the goodness of fit, are also listed. S, superior; I, inferior; T, temporal; N, nasal.

plateau value extracted from exponential fit to the data was used to normalize initial TPF values extracted from the straight line fit.

$$TPF(\Delta t_{dark}) = \frac{Initial\ TPF\ from\ straight\ line\ fit}{Plateau\ value\ from\ exponential\ fit}$$

The rationale for normalizing to the plateau value is based on the MLP model for pigment kinetics during steady state illumination.[44] According to this model, regardless of the pigment fraction available at $t = 0$, pigment regeneration and bleaching eventually are expected to reach an equilibrium value. Thus, the equilibrium value could be used to normalize out any absolute differences in image quality between different videos for the same data set from the same retinal location. Time constants for these normalized dark adaptation data were extracted by curve fitting to the exponential function, $f(x) = a \times exp(-bx) + c$ using MATLAB. Exponential fits were chosen for their simplicity.

Results

Two-Photon Autofluorescence From Photoreceptors

Two-photon fluorescence from a well-defined mosaic of cells was visualized in the outer retina. At various eccentricities, the sizes, densities, and distribution of these cells resembled the corresponding features of rod and cone photoreceptor cells imaged in the reflectance mode. An image of the light backscattered from photoreceptor mosaic in the peripheral retina recorded in confocal modality (also referred to as reflectance image) is shown in Figure 3a and the corresponding two-photon image from the same location is shown in Figure 3b. All cones in the reflectance image can be seen in the two-photon image. Additionally, many single rods were visible in the reflectance as well as two-photon image, although all rods are not visibly distinguishable. Similar to the modal pattern exiting a waveguide dominated by the lowest order mode,[48] dark halos were visible in the reflectance images. Dark halos around individual cells also were visible in the TPF images from the same set of cone photoreceptors. Images also were recorded at a location in the parafoveal retina and individual cone photoreceptors were visible in the reflectance (Fig. 3c) as well as fluorescence image (Fig. 3d). Low spatial variations in image intensity are likely related to the retinal vasculature or choroid and are observed routinely in adaptive optics imaging.

TPF During Exposure to the Imaging Beam Alone

As described in the Methods section, after allowing the retina to dark adapt for 35 minutes, TPF was recorded from cones and rods over time. With the onset of light, the magnitude of autofluorescence from photoreceptors increased monotonically with time and then plateaued, as shown in Figure 4a for rods and Figure 4b for cones.

When cones were imaged with high light intensity (7 mW), fluorescence increased rapidly. After this initial increase, fluorescence usually peaked between 5 and 20 seconds and then gradually declined and then plateaued. Compared to expected rate of photopigment bleaching, the fluorescence rise was slower, as shown in Figure 4c.

Time Course of TPF at Different Stages of Dark Adaptation

Time courses of TPF from the same retinal location, for six variable periods of time in the dark (or dark-intervals, Δt_{dark}) following visible stimulation are shown in Figures 5a and 5b; TPF for the $\Delta t_{dark} = 0$ minute time point (imaged immediately after bleach) decreased monotonically and eventually plateaued. In contrast, the TPF profile recorded at $\Delta t_{dark} = 30$ minutes time point (or 30 minutes in the dark after bleach before recording TPF) increased gradually and plateaued. Intermediate time points between these two extreme cases gave rise to the family of curves shown in Figures 5a and 5b. Peak fluorescence responses occurred either at the beginning of the recorded video or at the end, thus highlighting the monotonic nature of their kinetics under our imaging conditions.

For rods, Δt_{dark} less than 2 minutes (0–2 minutes after bleach or 0%–20% of the initially available photopigment), TPF decreased with time and plateaued, whereas for Δt_{dark} greater

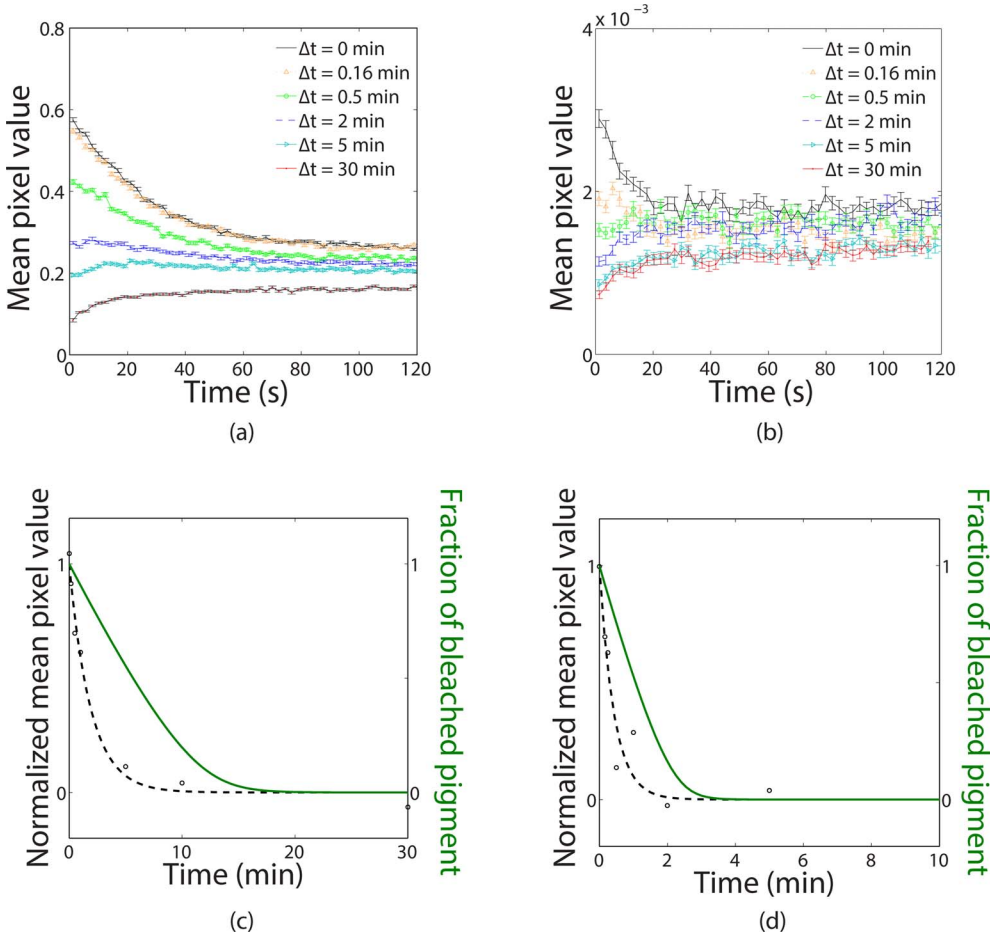

Figure 5. Two-photon fluorescence response of the retina during different stages of dark adaptation. (**a**) Two-photon fluorescence responses for rods recorded after variable periods of time in dark following a strong photopic bleach at 565 nm. Different curves correspond to different Δt_{dark} periods after which fluorescence was recorded (see *legend*) with 7 mW incident light at a location 4.86 mm superior and temporal relative to the center of the foveal avascular zone. (**b**) Two-photon fluorescence responses from cones recorded after variable periods of time in the dark following a strong photopic bleach at 565 nm. Different curves correspond to different Δt_{dark} periods after which fluorescence was recorded (see *legend*) with 750 μW incident light at a location 0.6 mm nasal to the center of the foveal avascular zone. Plots of initial TPF values from (**a**) and (**b**), normalized to plateau values, as a function of time in the dark are shown in (**c**) and (**d**), respectively, as *open circles*. The *dashed lines* in (**c**) and (**d**) are the exponential fits to the data. Inverse plots of photopigment density during regeneration in the dark after bleach, are shown for rods in (**c**) and for cones in (**d**). These were calculated using the MLP model[44] using parameters described in text.

than 5 minutes (>5 minutes after bleach or 45%–100% of the initially available photopigment), fluorescence increased from lower values and then plateaued (Fig. 5a). This suggests that the inflection point for the concavity of these profiles occurred between 2 and 5 minutes for light levels used for our imaging, although the temporal sampling was insufficient to capture this detail.

For cones, with Δt_{dark} less than or equal to 10 seconds (0–10 seconds after bleach or 0%–8% IAP), TPF decreased with time, whereas for Δt_{dark} greater than 30 seconds (>30 seconds after bleach or 24%–100% IAP), fluorescence increased from lower values. The inflection point for the concavity of cone TPF profiles occurred between 10 and 30 seconds for these light levels (Fig. 5b).

Initial TPF signal levels decreased with the duration of dark intervals after bleaching. Normalized curves for the initial TPF are shown in Figures 5c and 5d for rods and cones, respectively, along with exponential fits to these data. For comparison, time courses of decreasing fluorescence in the dark in rods and cones have been plotted along with the expected regeneration kinetics of their respective photopigment (shown in green in Figs. 5c, 5d). Fluorescence from rods and cones decreased approximately 3 to 4 times faster than the expected regeneration rate of their photopigment. Moreover, the rate of decreasing fluorescence from cones was approximately 4 times faster than the rate of decline in rod fluorescence. This ratio is similar to the ratio of the rates of pigment regeneration in the dark reported previously for cones and rods.[15,45] Table 1 lists the time constants obtained by curve fitting.

Adaptation to Spectrally Dissimilar Stimuli Reveals Visually Distinct Subsets of Cells

The distribution of two-photon autofluorescence from a mosaic of cells was not homogeneous. In some cases after a short period of photopic exposure, a sparsely distributed subset of cells that was dimmer than the rest of the mosaic could be distinguished. An example of this phenomenon was produced with the imaging protocol described in the section Adaptation to Spectrally Dissimilar Stimuli above, and is shown in Figures 6a and 6b. The TPF image shown in Figure 6a was

Investigative Ophthalmology & Visual Science

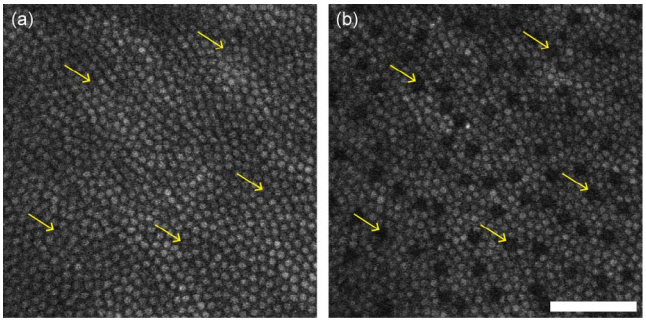

Figure 6. Two-photon fluorescence image of cone photoreceptors collected immediately after bleach at 420 nm are shown in (**a**). Two-photon fluorescence image of the same set of cones recorded immediately after bleach at 565 nm are shown in (**b**). *Arrows* point to the same cells in the images shown in (**a**) and (**b**). Both fluorescent images were recorded with 7 mW light at 0.73 mm inferior to the fovea. *Scale bar*: 50 μm.

collected immediately after a full-field bleach at 420 nm. The image shown in Figure 6b was collected at the same location as Figure 6a after stimulation with 565 nm light and a subset of cones were relatively dimmer than the majority of cells. These dim cells comprised 8% of the total population of cells in this sample and their density was 2200 cells/mm^2. These numbers are similar to the expected fraction and density of S cones at this retinal eccentricity (see Table 2), suggesting that the sparse mosaic of cells seen in Figure 6b are S cones.

Discussion

We developed a custom in vivo two-photon ophthalmoscope for retinal imaging in primates (Fig. 1) that allows the separation of functional responses from rod and cone photoreceptors. Supplementing previous studies using rodents,[28–31] this contribution is of interest because time-variable autofluorescence could be a functional marker for monitoring physiological activity at a cellular scale with potential diagnostic applications in humans. The use of this modality is limited by the sensitivity and specificity of its detection. Although sensitivity is a concern, the focus of the current investigation was to examine the specificity of two-photon imaging as a functional imaging tool because the identity of the dominant fluorophore(s) contributing to this time-variable fluorescence in the outer retina is uncertain. Ex vivo spectroscopy of sources of fluorescence in photoreceptors has confirmed the presence of all-*trans*-retinol in the outer segments, and metabolites, such as NAD(P)H, in the inner segments,[20,21,29,30,49] but other candidate molecules also could be responsible, such as all-*trans*-retinal, FAD,[49] retinyl esters, lipofuscin precursors,[28–30,50] and perhaps others. Despite the variety of candidate fluorophores, some of them can be ruled out easily. In the outer retina, fluorescence from photoreceptors (Fig. 3) was greater than any autofluorescence from RPE cells at deeper focal planes (data not shown) and the RPE mosaic could not be visualized. This suggests that retinyl esters and lipofuscin cannot be the dominant source of time-variable autofluorescence shown in Figures 4 and 5.

Autofluorescence from pyridine dinucleotides, such as NADH, NADPH, and flavoproteins, such as FAD have been used to track neuronal metabolism.[51,52] In brain slices, synaptic activation leads to an initial decrease (1%–4%) in fluorescence from NADH followed by an increase (<10%) and eventually equilibrium is achieved.[53–55] Fluorescence of FAD is expected to be inverted relative to NAD(P)H.[51,56,57] However, we have found that the fractional increase in autofluorescence recorded from photoreceptors during light adaptation (Fig. 4) was considerably larger than the fractional changes measured in brain slices.[53,55] This suggests that these metabolites are not likely to be the dominant source of time-variable fluorescence from photoreceptors although they might contribute to baseline fluorescence.

Comparisons with photopigment kinetics suggest that retinoids are likely to be the dominant source of time-variable fluorescence in the retina. All-*trans*-retinol and not all-*trans*-retinal, is the most likely candidate within photoreceptors because of their relative two-photon excitation efficiencies at 730 nm excitation.[58,59] The following observations serve to support this claim.

Table 2. Distribution and Density of Putative S Cones Observed at Various Eccentricities in Multiple Animals Are Listed

Distance From Fovea, mm	Measured Density in this Study, Cells/mm^2	In Literature, Cells/mm^2
2.5	1150	800
3.1	706	600
1.5	1000	950
0.7	2200	~1200
1.8	1400	~800

Literature values from human retinas also are shown for comparison.[65]

Fluorescence Increased With Photopigment Bleaching

Ex vivo studies done with isolated frog photoreceptors,[20] mouse,[28] and primate retinas[32,50] have demonstrated an increase in the relative magnitude of TPF signals from photoreceptors upon exposure to stimulus. Consistent with these studies, we also have observed an increase in fluorescence from photoreceptors with the onset of stimulation from imaging beam after a sufficiently long period of dark adaptation, as shown in Figure 4. This is likely due to stimulation from the light source used for TPF excitation and agrees with the expectation that all-*trans*-retinol should be produced when photopigments are bleached, thereby increasing fluorescence.

The Rate of Increased Fluorescence Was Slower Than the Expected Rate of Photopigment Bleaching

Upon absorption of a photon by photopigments, intermediate metapigments are generated and all-*trans*-retinal is released from opsin, which then is reduced to all-*trans*-retinol.[5] Studies in isolated salamander cone photoreceptors have shown previously that under strong bleaching conditions (>90% bleach), fluorescence from retinol initially increases, peaks, and then declines.[24] Reportedly, this is because the rate of production of all-*trans*-retinol is greater than the rate of removal under these conditions.[22,23,60] As shown in Figure 4c, in the extreme case when cone photopigments were bleached instantly by the imaging beam, TPF peaked after a lag of approximately 5 to 20 seconds and the time profile of fluorescence was nonmonotonic. This is inconsistent with predictions from pigment bleaching calculations and suggests that rate of production of all-*trans*-retinol might be faster than the rate of clearance after an intense bleach.

Investigative Ophthalmology & Visual Science

During Dark Adaptation, Fluorescence Declined Faster Than the Expected Rate for Photopigment Regeneration

We observed a decrease in fluorescence during dark adaptation in rods and cones as shown in Figures 5c and 5d, and measured the rate of decline (Table 1). We found that fluorescence from rods and cones decreased approximately 4 times faster than the expected rate of pigment regeneration.[13] This observation is consistent with the retinoid hypothesis because if the fluorescent molecules involved are intermediate components of the retinoid cycle, then they should be cleared before the entire cycle can regenerate pigment. We also observed that cone pigment recovery was approximately four times faster than rod pigment recovery, consistent with photopigment densitometry.[15,45] These observations rule out the possible role of optical screening from photopigments or melanin as the cause of time-varying autofluorescence.

Fluorescence Profiles During Steady State Illumination Were Similar to Expected Photopigment Density Curves

The MLP model has been used to describe photopigment kinetics during steady state illumination[44] wherein the concavity of the pigment density response curve as a function of time depends on the initial pigment density and the amount of light stimulation. As expected, fluorescence changes related to all-*trans*-retinol production were inversely related to photopigment density (Figs. 5a, 5b). For the extreme case when the retina was exposed to strong light, the intensity of fluorescence was initially high. With pigments depleted, the molecules created as a result of stimulation would be cleared away as a part of the visual cycle, resulting in a decline in fluorescence as observed. Two-photon fluorescence eventually plateaued, possibly due to equilibrium between the continuous production and removal of all-*trans*-retinol. For the other extreme case, the retina was allowed to dark adapt after photo-bleaching for 30 minutes before recording and the opposite trend was observed. With the onset of imaging light, stimulation caused by the beam induced photoactivation, resulting in the production of fluorescent molecules. Moreover, continued pigment depletion due to stimulation from the imaging light was balanced by the regeneration process and, consequently, fluorescence stabilized and plateaued. All intermediate responses shown in Figures 5a and 5b can be explained by the steady state stimulation scenario described by the MLP model because different periods of recovery in the dark correspond to a variety of initial photopigment states. This affected the concavity of TPF curves under steady state stimulation, an interpretation consistent with the proposed hypothesis that all-*trans*-retinol is likely to be the dominant fluorophore under these experimental conditions.

Photoreceptors Minimally Stimulated by Infrared Light Appeared Dimmer

Using two-photon imaging, we observed sparse mosaics of dimmer cones in the primate retina. The density and distribution of these cones were similar to the known density and distribution of S cones in the primate retina at measured eccentricities (Table 2). The appearance of this dim mosaic of cones in the living eye under two-photon excitation (Fig. 6b) can be explained based on the spectral sensitivity differences between S and L/M cones. This is an extension of the idea that evoked fluorescence is related directly to photo-stimulation with subsequent production of retinoids that allows detection of S cones based on their spectral sensitivity.

The above observations support the claim that all-*trans*-retinol is the dominant source of time-variable fluorescence, with possibly some minor contributions from other metabolites. In the future, two-photon imaging could be used potentially to image the retinas of patients with visual cycle and metabolic defects. However, before that can be done, rigorous light safety studies must be conducted. Light levels used for imaging in Figure 4a were at least a factor of 9 above the safety limits prescribed by the American National Standards Institute,[61] but within the safety limits for data shown in Figure 4b and much lower than the light levels that can be expected to cause photobleaching of all-*trans*-retinol.[62] The retinal locations appeared slightly different after imaging for a few minutes but normal two-photon temporal responses could always be elicited from same retinal locations even week(s) later. However, we do acknowledge that any functional response reported here could be due to unknown damaging mechanisms from the severity of the light levels used. With further advances in technology, this imaging potentially can be done at lower and safer light levels. Infrared pulsed light sources also could impact the retina in other ways since exposure to pulsed light sources can heat up tissue due to absorption of energy by molecules, such as melanin, which are present in the eye as well as the skin.[63] This could cause a rise in temperature, distort the native physiology of the retina, and consequently affect measurement of the natural kinetics of the retinoid cycle. Factors, such as anesthesia and photoreversal, also could affect retinal imaging but their effects were not addressed in this study.

In summary, we have characterized the fluorescence responses emanating from individual photoreceptor cells in the primate retina and observed differences in the responses from rods and cones. Two-photon excitation also allows classification of S cones, which appear dimmer than other cones in the retinal mosaic. All-*trans*-retinol is the most likely candidate contributing to time-variable fluorescence, although nonnegligible contributions from metabolites, such as NAD(P)H and FAD, to time-variable fluorescence cannot be completely ruled out. Careful spectroscopic studies or pharmaceutical approaches for perturbing the Krebs cycle or the visual cycle in the living eye are needed to completely discern the contribution from all these molecules. With future improvements in imaging methodology, adaptive optics assisted in vivo two-photon imaging could be used for clinical diagnosis, vision evaluation, and functional testing in single cells of the living eye, thereby enabling early stratification of patients for more individualized and effective treatment.

Acknowledgments

The image acquisition software and firmware were developed by Qiang Yang, adaptive optics control software by Alfredo Dubra and Kamran Ahmad, and image registration software by Alfredo Dubra and Zachary Harvey. The stereotaxic cart design is courtesy of the United States Air Force, and was constructed by Martin Gira and Mark Ditz. Animals were handled by Lee Anne Schery, Tracy Bubel, Amber Walker, or Louis DiVincenti before and during experimentation. The authors thank Keith Parkins, Ethan Rossi, Jesse Schallek, Ge Song, Jessica Kraker, Sarah Walters, Joynita Sur, Jie Zhang, Benjamin Masella, and Ted Tweitmeyer for their contributions.

Supported by the National Eye Institute and the National Institute of Aging of the National Institutes of Health under Award Numbers R44 AG043645, R01 EY022371, R24 EY024864 and P30 EY001319, BRP-EY014375 and K23-EY016700. The content is solely the

responsibility of the authors and does not necessarily represent the official views of the National Institutes of Health. This study was also supported by an unrestricted grant to the University of Rochester Department of Ophthalmology from Research to Prevent Blindness, New York, New York, and by grants from the Arnold and Mabel Beckman Foundation. K.P. is John H. Hord Professor of Pharmacology.

Disclosure: **R. Sharma**, Polgenix, Inc. (F), P; **C. Schwarz**, Polgenix, Inc. (F); **D.R. Williams**, Polgenix, Inc. (F), Canon (F), P; **G. Palczewska**, Polgenix, Inc. (E); **K. Palczewski**, Polgenix, Inc. (C), P; **J.J. Hunter**, Polgenix, Inc. (F), P

References

1. Baumann C. Franz Boll. *Vision Res*. 1977;17:1267–1268.
2. Kühne W, Foster M. *On the Photochemistry of the Retina and on Visual Purple*. London: Macmillan and Co.; 1878.
3. Wald G. Carotenoids and the visual cycle. *J Gen Physiol*. 1935; 19:351–371.
4. Hubbard R, Wald G. Cis-trans isomers of vitamin A and retinene in the rhodopsin system. *J Gen Physiol*. 1952;36:269–315.
5. Wald G. Molecular basis of visual excitation. *Science*. 1968; 162:230–239.
6. Kiser PD, Golczak M, Palczewski K. Chemistry of the retinoid (visual) cycle. *Chem Rev*. 2014;114:194–232.
7. Palczewski K, Jager S, Buczylko J, et al. Rod outer segment retinol dehydrogenase: substrate specificity and role in phototransduction. *Biochemistry (Mosc)*. 1994;33:13741–13750.
8. Dowling JE. Chemistry of visual adaptation in the rat. *Nature*. 1960;188:114–118.
9. Das SR, Bhardwaj N, Kjeldbye H, Gouras P. Muller cells of chicken retina synthesize 11-cis-retinol. *Biochem J*. 1992;285: 907–913.
10. Mata NL, Radu RA, Clemmons RS, Travis GH. Isomerization and oxidation of vitamin A in cone-dominant retinas: a novel pathway for visual-pigment regeneration in daylight. *Neuron*. 2002;36:69–80.
11. Wang J-S, Kefalov VJ. An alternative pathway mediates the mouse and human cone visual cycle. *Curr Biol CB*. 2009;19: 1665–1669.
12. Wang J-S, Kefalov VJ. The cone-specific visual cycle. *Prog Retin Eye Res*. 2011;30:115–128.
13. Lamb TD, Pugh EN. Dark adaptation and the retinoid cycle of vision. *Prog Retin Eye Res*. 2004;23:307–380.
14. Campbell FW, Rushton WAH. Measurement of the scotopic pigment in the living human eye. *J Physiol*. 1955;130:131–147.
15. Rushton WA. Dark-adaptation and the regeneration of rhodopsin. *J Physiol*. 1961;156:166–178.
16. Van Norren D, van der Kraats J. A continuously recording retinal densitometer. *Vision Res*. 1981;21:897–905.
17. DeLint PJ, Berendschot TT, van de Kraats J, van Norren D. Slow optical changes in human photoreceptors induced by light. *Invest Ophthalmol Vis Sci*. 2000;41:282–289.
18. Grieve K, Roorda A. Intrinsic signals from human cone photoreceptors. *Invest Ophthalmol Vis Sci*. 2008;49:713–719.
19. Masella BD, Hunter JJ, Williams DR. New wrinkles in retinal densitometry. *Invest Ophthalmol Vis Sci*. 2014;55:7525–7534.
20. Chen C, Tsina E, Cornwall MC, Crouch RK, Vijayaraghavan S, Koutalos Y. Reduction of all-trans retinal to all-trans retinol in the outer segments of frog and mouse rod photoreceptors. *Biophys J*. 2005;88:2278–2287.
21. Kaplan MW. Distribution and axial diffusion of retinol in bleached rod outer segments of frogs (Rana pipiens). *Exp Eye Res*. 1985;40:721–729.
22. Ala-Laurila P, Kolesnikov AV, Crouch RK, et al. Visual cycle: dependence of retinol production and removal on photoproduct decay and cell morphology. *J Gen Physiol*. 2006;128:153–169.
23. Chen C, Blakeley LR, Koutalos Y. Formation of all-trans retinol after visual pigment bleaching in mouse photoreceptors. *Invest Ophthalmol Vis Sci*. 2009;50:3589–3595.
24. Dacey D. Origins of perception: retinal ganglion cell diversity and the creation of parallel visual pathways. In: Gazzaniga MS, ed. *The Cognitive Neurosciences*. 3rd ed. Cambridge, MA: MIT Press; 2004:281–301.
25. Dillon J, Zheng L, Merriam JC, Gaillard ER. Transmission spectra of light to the mammalian retina. *Photochem Photobiol*. 2007;71:225–229.
26. Göppert M. Über die Wahrscheinlichkeit des Zusammenwir kens zweier Lichtquanten in einem Elementarakt. *Naturwissenschaften*. 1929;17:932–932.
27. Denk W, Strickler JH, Webb WW. Two-photon laser scanning fluorescence microscopy. *Science*. 1990;248:73–76.
28. Imanishi Y, Batten ML, Piston DW, Baehr W, Palczewski K. Noninvasive two-photon imaging reveals retinyl ester storage structures in the eye. *J Cell Biol*. 2004;164:373–383.
29. Palczewska G, Maeda T, Imanishi Y, et al. Noninvasive multiphoton fluorescence microscopy resolves retinol and retinal condensation products in mouse eyes. *Nat Med*. 2010; 16:1444–1449.
30. Palczewska G, Dong Z, Golczak M, et al. Noninvasive two-photon microscopy imaging of mouse retina and retinal pigment epithelium through the pupil of the eye. *Nat Med*. 2014;20:785–789.
31. Maeda A, Palczewska G, Golczak M, et al. Two-photon microscopy reveals early rod photoreceptor cell damage in light-exposed mutant mice. *Proc Natl Acad Sci U S A*. 2014; 111:E1428–E1437.
32. Hunter JJ, Masella B, Dubra A, et al. Images of photoreceptors in living primate eyes using adaptive optics two-photon ophthalmoscopy. *Biomed Opt Express*. 2011;2:139–148.
33. Richards-Kortum R, Sevick-Muraca E. Quantitative optical spectroscopy for tissue diagnosis. *Annu Rev Phys Chem*. 1996;47:555–606.
34. Zipfel WR, Williams RM, Christie R, Nikitin AY, Hyman BT, Webb WW. Live tissue intrinsic emission microscopy using multiphoton-excited native fluorescence and second harmonic generation. *Proc Natl Acad Sci U S A*. 2003;100:7075–7080.
35. Berezin MY, Achilefu S. Fluorescence lifetime measurements and biological imaging. *Chem Rev*. 2010;110:2641–2684.
36. Sobotka H, Kann S, Loewenstein E. The fluorescence of vitamin A. *J Am Chem Soc*. 1943;65:1959–1961.
37. Gómez-Vieyra A, Dubra A, Malacara-Hernández D, Williams DR. First-order design of off-axis reflective ophthalmic adaptive optics systems using afocal telescopes. *Opt Express*. 2009;17:18906–18919.
38. Dubra A, Sulai Y. Reflective afocal broadband adaptive optics scanning ophthalmoscope. *Biomed Opt Express*. 2011;2: 1757–1768.
39. Gu M, Sheppard CJR. Comparison of three-dimensional imaging properties between two-photon and single-photon fluorescence microscopy. *J Microsc*. 1995;177:128–137.
40. Griffin DR, Hubbard R, Wald G. The sensitivity of the human eye to infra-red radiation. *J Opt Soc Am*. 1947;37:546.
41. Palczewska G, Vinberg F, Stremplewski P, et al. Human infrared vision is triggered by two-photon chromophore isomerization. *Proc Natl Acad Sci*. 2014;111:E5445–E5454.

42. Baylor DA, Nunn BJ, Schnapf JL. The photocurrent, noise and spectral sensitivity of rods of the monkey Macaca fascicularis. *J Physiol*. 1984;357:575–607.
43. Baylor DA, Nunn BJ, Schnapf JL. Spectral sensitivity of cones of the monkey Macaca fascicularis. *J Physiol*. 1987;390:145–160.
44. Mahroo O, Lamb T. Recovery of the human photopic electroretinogram after bleaching exposures: estimation of pigment regeneration kinetics. *J Physiol*. 2004;554:417–437.
45. Rushton WA, Henry GH. Bleaching and regeneration of cone pigments in man. *Vision Res*. 1968;8:617–631.
46. Morgan JIW, Pugh EN Jr. Scanning laser ophthalmoscope measurement of local fundus reflectance and autofluorescence changes arising from rhodopsin bleaching and regeneration. *Invest Ophthalmol Vis Sci*. 2013;54:2048–2059.
47. Dubra A, Harvey Z. Registration of 2D images from fast scanning ophthalmic instruments. In: Fischer B, Dawant BM, Lorenz C, eds. *Biomedical Image Registration. Lecture Notes in Computer Science*. Springer Verlag: Berlin Heidelberg; 2010:60–71.
48. Enoch JM. Wave-guide modes in retinal receptors. *Science*. 1961;133:1353–1354.
49. Zhao L, Qu J, Niu H. Identification of endogenous fluorophores in the photoreceptors using autofluorescence spectroscopy. *Proc. SPIE: Optics in Health Care and Biomedical Optics III*. 2008;6826:682614.
50. Palczewska G, Golczak M, Williams DR, Hunter JJ, Palczewski K. Endogenous fluorophores enable two-photon imaging of the primate eye. *Invest Ophthalmol Vis Sci*. 2014;55:4438–4447.
51. Chance B, Cohen P, Jobsis F, Schoener B. Intracellular oxidation-reduction states in vivo. *Science*. 1962;137:499–508.
52. Harrison DE, Chance B. Fluorimetric technique for monitoring changes in the level of reduced nicotinamide nucleotides in continuous cultures of microorganisms. *Appl Microbiol*. 1970; 19:446–450.
53. Lipton P. Effects of membrane depolarization on nicotinamide nucleotide fluorescence in brain slices. *Biochem J*. 1973;136: 999–1009.
54. Shuttleworth CW, Brennan AM, Connor JA. NAD(P)H fluorescence imaging of postsynaptic neuronal activation in murine hippocampal slices. *J Neurosci*. 2003;23:3196–3208.
55. Kasischke KA, Vishwasrao HD, Fisher PJ, Zipfel WR, Webb WW. Neural activity triggers neuronal oxidative metabolism followed by astrocytic glycolysis. *Science*. 2004;305:99–103.
56. Rosenthal M, Jöbsis FF. Intracellular redox changes in functioning cerebral cortex. II. Effects of direct cortical stimulation. *J Neurophysiol*. 1971;34:750–762.
57. Duchen MR, Surin A, Jacobson J. Imaging mitochondrial function in intact cells. *Methods Enzymol*. 2003;361:353–389.
58. Birge RR, Bennett JA, Pierce BM, Thomas TM. Two-photon spectroscopy of the visual chromophores. Evidence for a lowest excited 1Ag–like .pi..pi.* state in all-trans-retinol (vitamin A). *J Am Chem Soc*. 1978;100:1533–1539.
59. Birge RR, Bennett JA, Hubbard LM, et al. Two-photon spectroscopy of all-trans-retinal. Nature of the low-lying singlet states. *J Am Chem Soc*. 1982;104:2519–2525.
60. Wu Q, Blakeley LR, Cornwall MC, Crouch RK, Wiggert BN, Koutalos Y. Interphotoreceptor retinoid-binding protein is the physiologically relevant carrier that removes retinol from rod photoreceptor outer segments. *Biochemistry (Mosc)*. 2007; 46:8669–8679.
61. ANSI. American National Standard for Safe Use of Lasers ANSI Z136.1-2014. 2014.
62. Wu Q, Chen C, Koutalos Y. All-trans retinol in rod photoreceptor outer segments moves unrestrictedly by passive diffusion. *Biophys J*. 2006;91:4678–4689.
63. Masters BR, So PTC, Buehler C, et al. Mitigating thermal mechanical damage potential during two-photon dermal imaging. *J Biomed Opt*. 2004;9:1265–1270.
64. Bedggood P, Metha A. Variability in bleach kinetics and amount of photopigment between individual foveal cones. *Invest Ophthalmol Vis Sci*. 2012;53:3673–3681.
65. Curcio CA, Allen KA, Sloan KR, et al. Distribution and morphology of human cone photoreceptors stained with anti-blue opsin. *J Comp Neurol*. 1991;312:610–624.

Investigative Ophthalmology & Visual Science